https://doi.org/10.15407/ujpe64.5.415

V. SHMID,[1] A. PODOLIAN,[1] A. NADTOCHIY,[1] O. KOROTCHENKOV,[1]
B. ROMANYUK,[2] V. MELNIK,[2] V. POPOV,[2] O. KOSULYA [2]

[1] Taras Shevchenko National University of Kyiv, Faculty of Physics
(64/13, Volodymyrs'ka Str., Kyiv 01601, Ukraine; e-mail: shmdvi@gmail.com)
[2] V.E. Lashkaryov Institute of Semiconductor Physics, Nat. Acad. of Sci. of Ukraine
(41, Nauka Ave., Kyiv 03028, Ukraine)

PHOTOELECTRIC PROPERTIES OF SiGe FILMS COVERED WITH AMORPHOUS- AND POLYCRYSTALLINE-SILICON LAYERS

The deposition of thin layers of amorphous (a-Si) or polycrystalline (poly-Si) silicon onto the $Ge_{0.25}Si_{0.75}$ film already covering the surface of a crystalline silicon (c-Si) wafer is found to significantly reduce the magnitude of the negative surface photovoltage (SPV) generated in the $Ge_{0.25}Si_{0.75}$ film. At the same time, if the light penetration depth is sufficiently large, so that light penetrates into both the deposited layers and the near-surface region in the Si substrate, a positive SPV is observed within time intervals exceeding 10–20 μs after the light pulse terminates. It is also found that the saturation of the a-Si layer in the a-Si/$Ge_{0.25}Si_{0.75}$/c-Si heterostructure results in a substantial (by a factor of six) growth of the positive component of the SPV signal. This effect can be used while developing efficient solar components on the basis of a-Si/Ge_xSi_{1-x}/c-Si heterostructures.

K e y w o r d s: photovoltage, SiGe, a-Si, poly-Si.

1. Introduction

In recent years, the interest in the photoelectric properties of Ge/Si heterostructures, especially in a spectral range of 1.3–1.55 μm, has considerably grown. New types of photodetectors based on interband transitions in low-dimensional silicon and germanium heterojunctions are intensively developed. Such devices can be used in fiber-optic communication lines and in monitoring systems [1–3].

In addition, the interest in Ge/Si heterostructures reveals itself through the promising prospects of their application to solar energetics [4–7]. However, the technologies used for the manufacture of high-performance solar cells still extensively apply structures based on crystalline silicon (c-Si). It is known that dangling bonds at the c-Si surface behave as effective recombination centers and decrease the lifetime of charge carriers [8]. In order to increase the optical absorption coefficient and the lifetime of charge carriers, the front surface of solar cells on the basis of c-Si is usually covered with an antireflection passivation SiO_2 or Si_3N_4 layer [9, 10].

In an alternative approach, amorphous silicon (a-Si) can be used as a passivation layer on the c-Si surface [11–17]. In the cited works, it was emphasized, e.g., that a-Si/c-Si heterostructures have some advantages, in particular, a larger separation length for photogenerated charge carriers with opposite charge signs [18], when the charge carriers are repelled from the interface, which results in a reduction of the surface recombination rate.

Besides c-Si, solar cells fabricated from a-Si and polycrystalline silicon (poly-Si) are widely used as well [19–21]. However, poly-Si suffers from the pres-

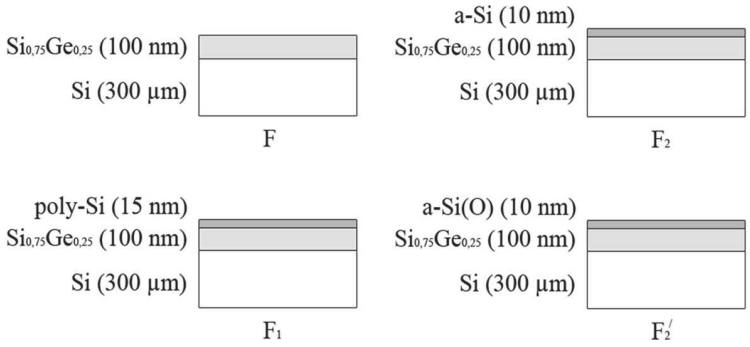

Fig. 1. Experimental samples: $Ge_{0.25}Si_{0.75}$/c-Si (F), poly-Si/$Ge_{0.25}Si_{0.75}$/c-Si (F_1), a-Si/$Ge_{0.25}Si_{0.75}$/c-Si (F_2), and a-Si(O)/$Ge_{0.25}Si_{0.75}$/c-Si (F'_2)

ence of grain boundaries, which worsen its electrical and optical properties and affect the device efficiency. In the case of poly-Si, this efficiency in many respects depends on the charge transfer properties, which are restricted by inter-grain potential barriers and defect states. In order to reduce the influence of those states, the latter can be passivated, e.g., by the plasma hydrogenation [22–25] or by the treatment in H_2O vapor [26].

At the same time, there are practically no works devoted to the study of the specific features of the photoelectric conversion in Ge/Si heterostructures. The available reports deal with the improvement of the energy conversion efficiency in the double heterojunction a-Si/c-Ge_xSi_{1-x}/c-Si [27], a reduction of the recombination rate in the n-$Si_{0.85}Ge_{0.15}$/p-c-Si structure, when the upper layer is coated with a passivation film of hydrogenated a-Si:H [28], and the processes of over-barrier activation of charge carriers at heterojunctions in the a-Si/c-Ge_xSi_{1-x}/p-c-Si structure [29]. In our previous study [30], we demonstrated a significant increase of the photovoltage magnitude in the structure "Ge_xSi_{1-x} nanoislands/c-Si," when the silicon-germanium layer was coated with a passivation a-Si film.

Therefore, the aim of this work is to study the photovoltage in the structures composed of a 100-nm $Ge_{0.25}Si_{0.75}$ layer on a c-Si substrate and coated with an a-Si or poly-Si film.

2. Samples and Experimental Technique

Samples of $Ge_{0.25}Si_{0.75}$/c-Si were fabricated using the method of epitaxial building-up – Low Pressure (Rapid Thermal) Chemical Vapor Deposition [LP (RT) CVD] – of a specially undoped 100-nm silicon-germanium layer on a Cz–Si(100) substrate of the p-type with a resistivity of about 10 Ω cm (sample F). Afterward, the $Ge_{0.25}Si_{0.75}$ layer was covered with a film of intentionally undoped amorphous silicon (a-Si) 10 nm in thickness (sample F_2). The deposition was carried out at a temperature of 520 °C using the method of plasma enhanced chemical vapor deposition (PECVD). Some of F_2 samples were heated up at a temperature of 400 °C for 5 min in the oxygen atmosphere (sample F_2). In order to create a film on the basis of poly-Si, some of samples F were covered within the PECVD method with a layer of intentionally undoped amorphous silicon 15 nm in thickness. Then they were annealed at a temperature of 640 °C. In the course of annealing, the a-Si film crystallized into the poly-Si one (sample F_1). All samples that were used in measurements are presented in Fig. 1.

The distribution of the germanium concentration across the $Ge_{0.25}Si_{0.75}$ layer was analyzed with the help of a flight-time mass spectrometer Ion-Tof-SIMS IV, by sputtering the surface making use of oxygen ions with a beam energy of 1 keV. A necessity of this control is associated with the fact that the temperature annealing of, e.g., sample F_1 may lead to the smearing of the $Ge_{0.25}Si_{0.75}$/c-Si heterointerfaces due to the germanium diffusion. In the course of previous studies dealing with the growth of thin Ge_xSi_{1-x} layers on silicon substrates at a temperature of about 700 °C, it was found that this diffusion may be substantial, especially in the field of spatially inhomogeneous deformations [31]. The results exhibited in Fig. 2 testify to the absence of the germanium diffusion into a poly-Si film in our samples.

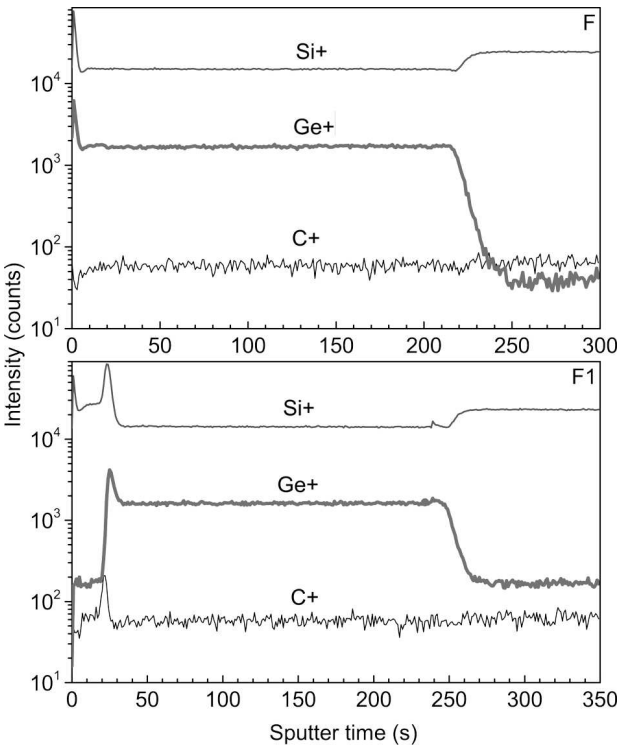

Fig. 2. Profiles of silicon, germanium, and carbon impurity distributions in samples F (upper panel) and F_1 (lower panel). The peaks at the $Ge_{0.25}Si_{0.75}$/Si heterointerface are associated with an enhanced sensitivity of the method in this region

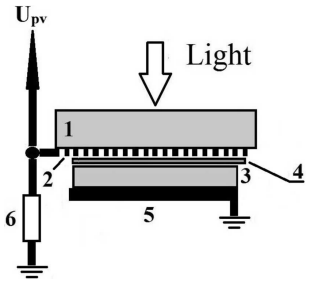

Fig. 3. Schematic diagram of the experimental installation: glass (*1*), translucent electrode (*2*), sample (*3*), mica (*4*), pressure contact (*5*), load resistance (*6*)

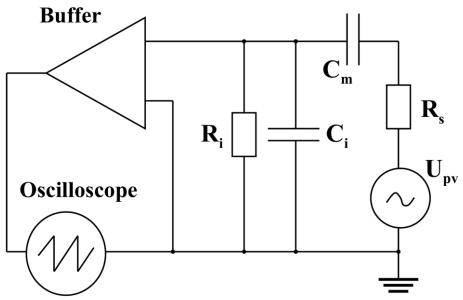

Fig. 4. Electric circuit allowing the relation between between the photovoltage signal value (U_{PV}) and the output of the amplifier to derive. R_s is the sample resistance, R_i the load resistance, C_m the capacitance between the sample and the electrode, and C_i is the input capacitance of the amplifier

The experimental setup for measuring the surface photovoltage is shown in Fig. 3. The photovoltage signal was generated with the help of semiconductor light-emitting diodes (LEDs) with two maxima in the radiation emission spectra: at $\lambda_p = 400$ and 870 nm. Rectangular pulses of the LED supply voltage 1 ms in duration were generated making use of a generator G5-54. It is known that light with a wavelength of about 400 nm is strongly absorbed by a-Si and poly-Si films: the light penetration depth $\alpha^{-1} \approx 30$ nm, where α is the optical absorption coefficient [32]. Light is also strongly absorbed in the $Ge_{0.25}Si_{0.75}$ layer (the light penetration depth is about 20 nm) [33]. As a result, the nonequilibrium charge carriers will be predominantly generated in a thin layer in vicinities of the a-Si/$Ge_{0.25}Si_{0.75}$ and poly-Si/$Ge_{0.25}Si_{0.75}$ heterojunctions. At the same time, light with the wavelength $\lambda_p = 870$ nm is less absorbed in a-Si, poly-Si, $Ge_{0.25}Si_{0.75}$, and c-Si (the light penetration depth is about 15 μm) and induces the almost uniform excitation of nonequilibrium charge carriers in the $Ge_{0.25}Si_{0.75}$ layer, i.e. in vicinities of both heterojunctions formed at the boundaries of the $Ge_{0.25}Si_{0.75}$ layer.

Light passes through glass, the translucent electrode, and mica and achieves the sample. Between the sample and the translucent electrode, there is a thin mica layer about 20 μm in thickness, which forms a plane condenser. The sample is fixed with the help of a grounded pressure contact. The signal obtained from the translucent electrode is amplified and sent to an oscilloscope. The load resistance before the amplifier was 1 GΩ. To prevent the influence of external factors on registering electronics, the measuring cell was arranged in a metal screening box.

The magnitude of the output signal can be related to the surface photovoltage signal using the equivalent circuit scheme depicted in Fig. 4. The calculation gives the following formula describing the relationship between the output signal values of the amplifier, ΔU,

and the photovoltage signal:

$$\Delta U = (\omega C_m R_i U_{\rm PV})/(\omega C_m R_s +$$

$$+\omega C_i R_i + \omega C_m R_i + i(\omega^2 C_i C_m R_i R_s - 1)),$$

where i is the imaginary unit, and ω the cyclic frequency of light modulation.

The obtained signal ΔU was read from the oscilloscope screen. Afterward, the curves of the photovoltage decrease were processed on a computer.

In order to study the change of the photovoltage kinetics with the change of light intensity using the integrating sphere method, the dependence of the radiation emission power of the LEDs on their supply current was studied, which showed a fairly good linear characteristic. This dependence revealed a rather exact linear behavior.

3. Experimental Results and Their Discussion

The formation of the photovoltage signal is known to occur owing to the spatial separation of non-equilibrium electrons and holes (e^- and h^+, respectively, in Fig. 5) by the field arising in the near-surface region of the space charge in the semiconductor. In this case, the energy band bending in the near-surface layer (the dotted curves in Fig. 5) decreases. It is evident that, together with the growth of the incident light intensity, the generation rate of non-equilibrium electrons and holes will also increase, which will be accompanied by an increase in the magnitude of the photovoltage signal and by a smaller band bending. One should expect that, starting from a certain incident light intensity, the generation rate of non-equilibrium charge carriers will reach such a value, at which the energy bands will be completely straightened (solid horizontal lines in Fig. 5) [34]. In this case, the magnitude of the photovoltage signal will reach its maximum value $U_{\rm PVsat}$ (see Fig. 5), and the latter will not increase, if the photogenerating light intensity grows further. The maximum value of the photovoltage signal and its sign determine the absolute value of the equilibrium band bending and the direction of this bending, respectively. In particular, in the situation depicted in Fig. 5, electrons will be localized under the semiconductor surface (arrow 2). But if the direction of a band bending is opposite, the accumulation of holes in the near-surface region will be observed.

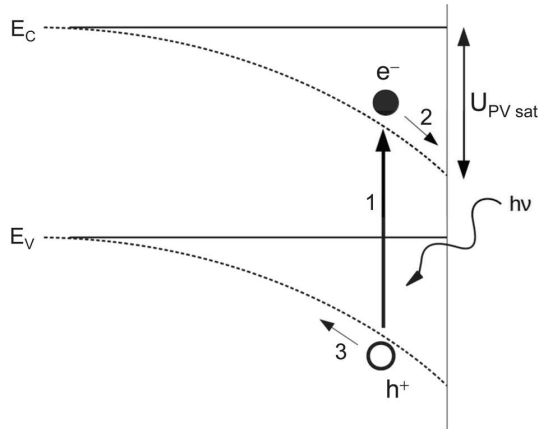

Fig. 5. Schematic diagram explaining the appearance of a surface photovoltage in the semiconductor located to the left from the vertical line. E_C and E_V are the edges of the conduction and valence, respectively, bands. As a result of the absorption of photons with the energy $h\nu$ (process 1), free electrons (e^-) and holes (h^+) are generated. Due to the existence of a space charge in the near-surface region and the corresponding band bending (dotted curves), e^- and h^+ become spatially separated in the processes indicated by arrows *2* and *3*. The energy $U_{\rm PV\,sat}$ corresponds to to the photovoltage value in the saturation state, which is observed at high light intensities, when the band bending is completely compensated (solid horizontal lines)

However, this method of determining the band bending can be applied relatively easily only to structures, in which the photovoltage signal is formed at a single interface (e.g., near the surface, see Fig. 5). But if a semiconductor structure – each of the structures examined in this work can be taken as an example – has a few interfaces (heterojunctions and the surface), the separation of non-equilibrium carriers at each interface will give its own contribution to the resulting photovoltage magnitude.

For instance, a schematic diagram in Fig. 6 demonstrates a band structure for sample F. It was plotted taking into account that the Ge_xSi_{1-x}/Si heterojunction is formed as a junction of the second kind [35, 36]. It is clear that if light is absorbed in the near-surface region (at $\lambda_p = 400$ nm under our experimental conditions), electrons e^- that are photoexcited in processes 1 and $1'$ can be localized in the energy minima both in the near-surface region (arrow 2) and at the surface of the Si substrate (arrow $2'$). In both cases, holes h^+ will be accumulated in the depth of the Ge_xSi_{1-x} layer (arrows $2''$). As a result, there arise two ambipolar components of the photovoltage

signal, $-U_{\rm PV1}$ and $+U_{PV2}$ in Fig. 6, with different relaxation times. The resulting value of the photovoltage signal equals $U_{PV} = -U_{PV1} + U_{PV2}$. However, if light (at $\lambda_p = 400$ nm in our case) penetrates into the Si substrate and is absorbed at a larger depth, the processes of electron and hole photoexcitation (they are designated by arrow $1''$ in Fig. 6) also take place. The concentration of holes in the Ge_xSi_{1-x} layer depth will be higher owing to their displacement from the Si substrate (arrow $2'''$ in Fig. 6). As a result, the photovoltage signal component $+U_{PV2}$ will substantially increase in comparison with the case where light is absorbed in the near-surface region only.

In addition, each of the terms $-U_{\rm PV1}$ and $+U_{\rm PV2}$ will be maximized with the corresponding straightening of the band bending at various photogenerating light intensities. It is clear that the presence of an additional a-Si or poly-Si layer on the structure surface in samples F_1, F_2, and F_2' makes the situation even more complicated. This means that the limiting value of the resulting photovoltage signal ($U_{\rm PV\,sat}$ in Fig. 5) cannot be used for the determination of the equilibrium band bending at each interface.

Taking those facts into account, we selected the intensity of photogenerating light that satisfies the condition of low level excitation, but at which the variation of the band bending induced by the illumination at each interface is much smaller than the equilibrium band bending.

A typical modification in the photovoltage kinetics depending on the light power in the selected power intervalis illustrated in Fig. 7. The presented curves of the photovoltage signal recession are well approximated by the bi-exponential law $|U_{\rm PV}| = U_1 \exp(-t/\tau_1) + U_2 \exp(-t/\tau_2)$ with the relaxation time constants τ_1 and τ_2 quoted in Table 1. The obtained data testify that a change in the light radiation intensity practically does not affect the form of the photovoltage kinetics (close values of relaxation times in Table 1 for various illumination powers). Furthermore, there is no saturation of the photovoltage signal intensity in the examined power(P) interval (see the inset in Fig. 7).

The time dependences of the photovoltage signal recession, which were registered for various experimental samples after the switching-off of the illumination with $\lambda_p = 400$ and 870 nm, are shown in Figs. 8 and 9, respectively. One can see that, in the case of photoexcitation with the wavelength $\lambda_p = 400$ nm,

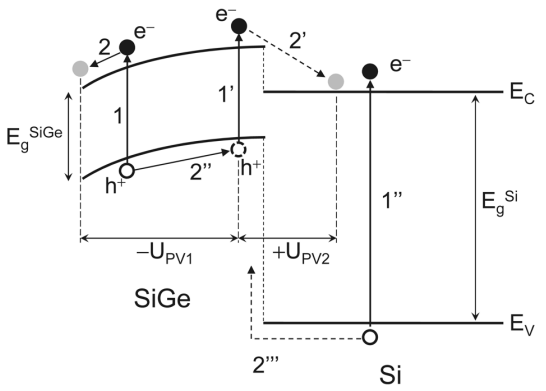

Fig. 6. Band diagram of the $Ge_{0.25}Si_{0.75}$/c-Si heterostructure (sample F) and the probable photo-induced processes of charge separation. The bending of the E_C- and E_V-bands at the $Ge_{0.25}Si_{0.75}$ surface (on the left in the figure) corresponds to the sign of a photovoltage registered at the illumination with $\lambda_p = 400$ nm. The band bending at the $Ge_{0.25}Si_{0.75}$/Si heterojunction is not taken into account

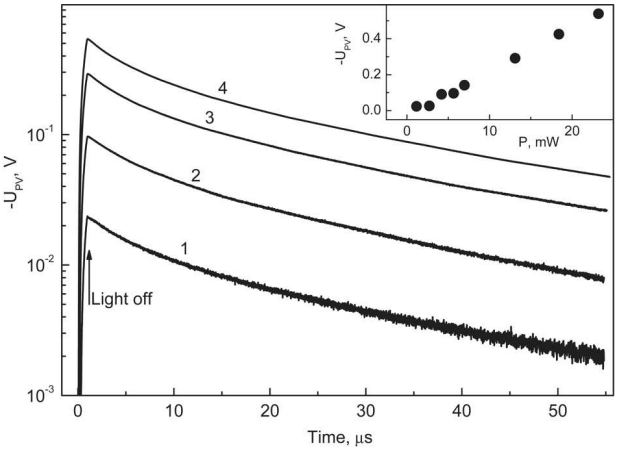

Fig. 7. Photovoltage kinetics in sample F at the excitation with 1-μs light pulses emitted by a light emitting diode with $\lambda_p = 400$ nm and at the powers: $P = 1.2$ (*1*), 4.2 (*2*), 13.1 (*3*), and 23.2 mW (*4*). The dependence of the peak photovoltage value at the moment when the light is switched-off (Light-off) on P is shown in the inset

Table 1. **Results of approximation of the data in Fig. 7 by a bi-exponential decay function**

LED power, mW	τ_1, μs	τ_2, μs
1.2 (curve *1*)	4.0 ± 0.1	21.2 ± 0.3
4.2 (curve *2*)	3.9 ± 0.1	21.5 ± 0.3
13.1 (curve *3*)	3.6 ± 0.1	20.7 ± 0.3
23.2 (curve *4*)	3.7 ± 0.1	21.0 ± 0.3

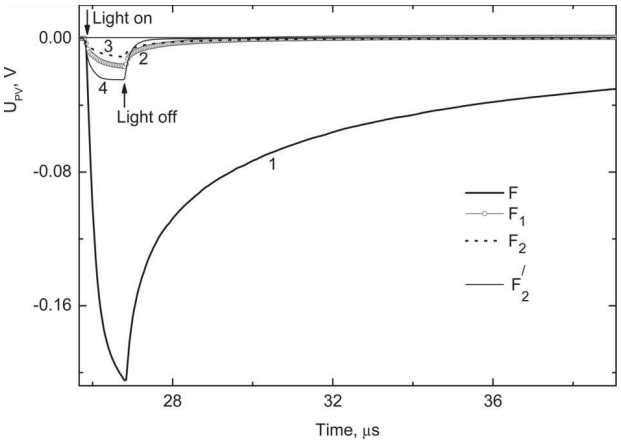

Fig. 8. Photovoltage kinetics in experimental samples F (*1*), F_1 (*2*), F_2 (*3*), and F'_2 (*4*) at their excitation with 1-μs light pulses from a light emitting diode with $\lambda_p = 400$ nm

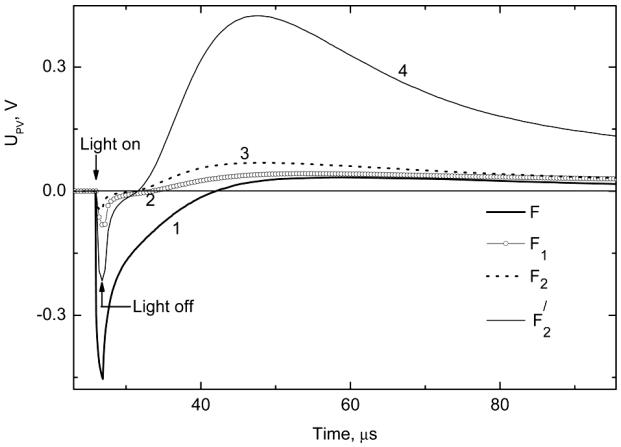

Fig. 9. Photovoltage kinetics in experimental samples F (*1*), F_1 (*2*), F_2 (*3*), and F'_2 (*4*) at their excitation with 1-μs light pulses from a light emitting diode with $\lambda_p = 870$ nm

Table 2. **Results of approximation of data in Fig. 8 by a bi-exponential decay function**

Sample	τ_1, μs	τ_2, μs
F	0.6 ± 0.1	5.6 ± 0.1
F_1	0.6 ± 0.1	–
F_2	0.6 ± 0.1	–
$F_2^{'}$	0.20 ± 0.05	–

the photovoltage signal becomes negative with the corresponding E_C- and E_V-band bending near the $Ge_{0.25}Si_{0.75}$ surface (see Fig. 6). In the initial sample F, the photovoltage signal amplitude is maximum (curve *1* in Fig. 8), and the rate of photovoltage recession is the slowest (the kinetics is the most hindered in this curve).

The deposition of the poly-Si and a-Si films (samples F_1 and F_2, respectively) leads to a considerable reduction of the photovoltage signal amplitude: by a factor of 12 for the poly-Si film and by a factor of 19 for the a-Si film in comparison with the corresponding value for sample F (compare curves *3* and *2* with curve *1* in Fig. 8). The kinetics of the photovoltage signal recession becomes also significantly accelerated.

For sample F'_2 covered with an oxygen-saturated a-Si film (curve *4* in Fig. 8), the amplitude of the photovoltage signal became more than twice as large as the corresponding value for sample F_2, when the a-Si film is not saturated with oxygen (curve *3* in Fig. 8). At the same time, the kinetics of the photovoltage recession is quicker for sample F'_2 in comparison with that for sample F_2.

The sections of the photovoltage signal recession in Fig. 8 were approximated by the sums of exponential curves. It turned out that the recession section for sample F is well approximated by the bi-exponential law, whereas, for samples F_1, F_2, and F'_2, by the monoexponential one. The recession time constants τ_1 and τ_2 calculated for those samples are quoted in Table 2.

If light with $\lambda_p = 870$ nm was used for illumination, the time dependences of the photovoltage signal became significantly complicated (curves *1–4* in Fig. 9). During the interval of the 1-μs light pulse action, the photovoltage signal monotonically increases by magnitude and reaches a negative peak value. After the exciting light has been switched-off, the photovoltage signal begins to decrease by magnitude down to a certain time moment, when it changes its sign from negative to positive. Afterward, the signal increases, reaches a maximum positive value, and then begins to decrease monotonically to zero.

After the deposition of a poly-Si (sample F_1, curve *2* in Fig. 9) or a-Si (sample F_2, curve *3* in Fig. 9) film, the negative peak value of the photovoltage signal under the illumination decreased by a factor of 5.5 or 10, respectively, in comparison with initial sample F (curve *1* in Fig. 9). The saturation of the a-Si film with oxygen (sample F'_2, curve *4* in Fig. 9) resulted in the growth of the negative peak value of the photovoltage signal by a factor of 4.5 in comparison

with sample F_2. When comparing the data depicted in Figs. 8 and 9, one can see that the film deposition and the treatment of samples in the oxygen atmosphere affect the negative section in the photovoltage relaxation curve in a similar way for both types of photoexcitation.

On the contrary, the positive component of the photovoltage depicted in Fig. 9 demonstrates a somewhat different tendency at the deposition of the poly-Si and a-Si films (the maximum positive values in curves *2* and *3* for samples F_1 and F_2, respectively, exceed the corresponding value in curve *1* for sample F). When the a-Si film is saturated with oxygen (sample F_2'), a significant (by a factor of 6 in comparison with sample F_2) growth of the photovoltage value in the positive section of curve *4* in Fig. 9 is observed.

It is evident that the difference between the photovoltage recession curves shown in Figs. 8 and 9 is associated with different light penetration depths into the samples at $\lambda_p = 400$ and 870 nm. As was mentioned above, this depth equals about 20 nm for $\lambda_p = 400$ nm and 15 μm for $\lambda_p = 870$ nm.

The schematic diagrams of band structures in samples F_1 and F_2, in which the results of previous researches [21, 37, 38] were taken into account, are plotted in Figs. 10 and 11. Similarly to sample F (Fig. 6), the excitation of charge carriers by light with $\lambda_p = 400$ nm, their separation giving rise to the photovoltage generation, and their recombination, which determines the photovoltage recession kinetics, predominantly take place at the a-Si/$Ge_{0.25}Si_{0.75}$ or poly-Si/$Ge_{0.25}Si_{0.75}$ heterojunction. Those photoexcitation processes are designated by arrows *1* and *1′* in Figs. 10 and 11. As a result, the negative photovoltage component marked as $-U_{PV1}$ in those figures will dominate. In the case of samples with the deposited poly-Si and a-Si films, a reduction of the photovoltage amplitude at the moment, when the light is switched-off, can be associated both with a decrease of the band bending near the $Ge_{0.25}Si_{0.75}$ surface (Fig. 6) occurring exactly owing to the film deposition and with the formation of rapid recombination centers for charge carriers in the poly-Si and a-Si layers and at the poly-Si/$Ge_{0.25}Si_{0.75}$ and a-Si/$Ge_{0.25}Si_{0.75}$ interfaces. For sample F_1, the latter effect is illustrated in Fig. 10, where arrows *3* and *4* designate the processes of electron capture onto the recombination centers (RCs) in the poly-Si layer and onto the interface states (ISs), and arrows *3′* and *4′* stand for the corresponding processes of hole capture.

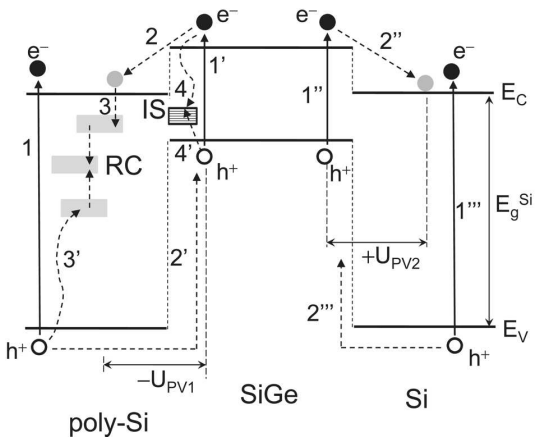

Fig. 10. Band diagram of the poly-Si/$Ge_{0.25}Si_{0.75}$/c-Si heterostructure (sample F_1) heterostructural band pattern. The notation RC means recombination centers in the poly-Si layer, and the notation IS stands for interface states at the poly-Si/$Ge_{0.25}Si_{0.75}$ interface

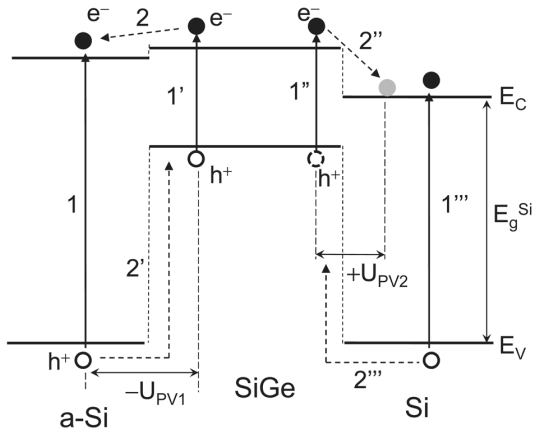

Fig. 11. Band diagram of the a-Si/$Ge_{0.25}Si_{0.75}$/c-Si heterostructure (sample F_2)

The data from Table 2 testify to the invariance of the fast component of the photovoltage recession with the relaxation time τ_1 in samples F, F_1, and F_2. But this component becomes significantly reduced after the a-Si film has been saturated with oxygen (sample F_2'). The initial sample F demonstrates a two-component kinetics (τ_1 and τ_2 in Table 2), which may testify to the existence of capture centers in the $Ge_{0.25}Si_{0.75}$ layer. On the other hand, the deposited poly-Si and a-Si layers generate

additional recombination centers in themselves and at the poly-Si/$Ge_{0.25}Si_{0.75}$ or a-Si/$Ge_{0.25}Si_{0.75}$ interface, which accelerates the photovoltage relaxation on the whole.

A matter of some interest is a growth of the photovoltage amplitude (curve *4* in Fig. 8) and a simultaneous reduction of the photovoltage relaxation time (τ_1 for sample F_2 in Table 2). Really, the photovoltage amplitude in the stationary case can be presented in the form [39]

$$U_{\rm PV}(0) \sim \frac{e\tau GL}{\varepsilon\varepsilon_0}, \quad (1)$$

where τ and G are the lifetime and the generation rate, respectively, of photo-excited charge carriers; L is the spatial separation length of nonequilibrium electrons e^- and holes h^+; ε_0 is the electric constant; and ε the dielectric constant. From this expression, it follows that the decrease of τ (and the corresponding decrease of τ_1 in Table 2) should be accompanied by a reduction of the photovoltage amplitude $U_{\rm PV}(0)$, which is not observed in sample F_2'. The annealing in the oxygen atmosphere evidently increases the magnitude of the product GL.

The excitation of charge carriers by light with $\lambda_p =$ = 870 nm and their separation and recombination take place at both heterojunctions: poly-Si/$Ge_{0.25}Si_{0.75}$ (or a-Si/$Ge_{0.25}Si_{0.75}$) and $Ge_{0.25}Si_{0.75}$/c-Si (arrows *1″* and *1‴* in Figs. 10 and 11). Just this circumstance is responsible for the emergence of the positive photovoltage component $+U_{\rm PV2}$, quite similarly to the photovoltage in sample F considered above (Fig. 6). The change of the photovoltage signal sign observed in this case can be explained by the fact that the recombination processes of nonequilibrium charge carriers in the near-surface layers of samples F, F_1, and F_2 are much faster than the recombination processes at the $Ge_{0.25}Si_{0.75}$/c-Si heterojunction. Furthermore, we may assume that, at the saturation of the a-Si film with oxygen, not only a reduction of the nonequilibrium charge carrier lifetime in a-Si takes place, but also the Fermi level in $Ge_{0.25}Si_{0.75}$ becomes partially shifted, which results in an increase of the band bending and the separation of non-equilibrium charge carriers (the increase of L in expression (1) for $U_{\rm PV}(0)$) at the $Ge_{0.25}Si_{0.75}$/c-Si heterojunction. As a result, starting from a certain time moment after the light has been switched-off, the positive component of a photovoltage signal begins to dominate over the negative component of the signal, so that the resulting positive photovoltage is generated (Fig. 9).

4. Conclusions

1. In this work, it is found that the $Ge_{0.25}Si_{0.75}$/c-Si, poly-Si/$Ge_{0.25}Si_{0.75}$/c-Si, a-Si/$Ge_{0.25}Si_{0.75}$/c-Si, and a-Si(O)/$Ge_{0.25}Si_{0.75}$/c-Si heterostructures excited by light pulses with a peak wavelength of 400 nm generate a monopolar negative photovoltage signal. If they are excited by light pulses with a peak wavelength of 870 nm, the generated photovoltage signal is bipolar.

2. The deposition of thin a-Si and poly-Si layers onto the surface of the $Ge_{0.25}Si_{0.75}$ layer leads to a significant reduction of the magnitude of the negative photovoltage-signal component and the acceleration of its relaxation rate, as well as to an insignificant growth of the magnitude of the positive photovoltage-signal component.

3. The saturation of the a-Si layer in the a-Si/$Ge_{0.25}Si_{0.75}$/c-Si heterostructure with oxygen gives rise to a substantial increase of the positive photovoltage-signal component. This effect can be used for the development of effective solar cells on the basis of the a-Si/Ge_xSi_{1-x}/c-Si heterostructure.

4. A model for the formation and relaxation of the positive and negative components of the photovoltage signal is proposed. According to it, the indicated processes are governed by the spatial separation and recombination of non-equilibrium charge carriers at heterojunctions that emerge at the interfaces of the $Ge_{0.25}Si_{0.75}$ layer with the Si substrate and the a-Si or poly-Si film. A substantial increase in the magnitude of the positive photovoltage-signal component in the a-Si/$Ge_{0.25}Si_{0.75}$/c-Si heterostructure with the oxygen-saturated a-Si layer can be explained, on the whole, by an increase of the band bending in the $Ge_{0.25}Si_{0.75}$ layer, which stimulates a more efficient separation of photogenerated electrons and holes in this layer.

1. A. Schüppen. SiGe-HBTs for mobile communication. *Solid-State Electron.* **43**, 1373 (1999).
2. K. Washio. SiGe HBT and BiCMOS technologies for optical transmission and wireless communication systems. *IEEE Trans. Electron. Dev.* **50**, 656 (2003).
3. Y. Iseri, H. Yamada, Y. Goda, T. Arakawa, K. Tada, N. Haneji. Analysis of electrorefractive index change in Ge/SiGe coupled quantum well for low-voltage silicon-based optical modulators. *Phys. E* **43**, 1433 (2011).

4. A. Alguno, N. Usami, T. Ujihara, K. Fujiwara, G. Sazaki, K. Nakajima, Y. Shiraki. Enhanced quantum efficiency of solar cells with self-assembled Ge dots stacked in multilayer structure. *Appl. Phys. Lett.* **83**, 1258 (2003).
5. H. Ferhati, F. Djeffal, Role of non-uniform Ge concentration profile in enhancing the efficiency of thin-film SiGe/Si solar cells. *Optik* **158**, 192 (2018).
6. X. Zhao, D. Li, T. Zhang, B. Conrad, L. Wang, A. H. Soeriyadi, J. Han, M. Diaz, A. Lochtefeld, A. Gerger, I. Perez-Wurfl, A. Barnett. Short circuit current and efficiency improvement of SiGe solar cell in a GaAsP-SiGe dual junction solar cell on a Si substrate. *Sol. Energ. Mater. Sol. Cell.* **159**, 86 (2017).
7. A.A. Shklyaev, V. A. Volodin, M. Stoffel, H. Rinnert, M. Vergnat. Raman and photoluminescence spectroscopy of SiGe layer evolution on Si(100) induced by dewetting. *J. Appl. Phys.* **123**, 015304 (2018).
8. A.G. Aberle, S. Glunz, W. Warta. Impact of illumination level and oxide parameters on Shockley–Read–Hall recombination at the Si-SiO_2 interface. *J. Appl. Phys.* **71**, 4422 (1992).
9. D. Diouf, J.P. Kleider, T. Desrues, P.-J. Ribeyron. Effects of the front surface field in n-type interdigitated back contact silicon heterojunctions solar cells. *Energ. Proc.* **2**, 59 (2010).
10. R. Pandey, R. Chaujar. Rear contact SiGe solar cell with SiC passivated front surface for >90-percent external quantum efficiency and improved power conversion efficiency. *Sol. Energy* **135**, 242 (2016).
11. *Physics and Technology of Amorphous-Crystalline Heterostructure Silicon Solar Cells*. Edited by W.G.J.H.M. van Sark, L. Korte, F. Roca (Springer, 2012) [ISBN: 978-3-642-22274-0].
12. *Amorphous Silicon/Crystalline Silicon Heterojunction Solar Cells*, edited by W.R. Fahrner (Chemical Industry Press and Springer, 2013) [ISBN: 978-3-642-37038-0].
13. S. Dauwe, J. Schmidt, R. Hezel. Very low surface recombination velocities on p- and n-type silicon wafers passivated with hydrogenated amorphous silicon films. In *Proceedings of the 29th IEEE Photovoltaic Specialists Conference, New Orleans, Louisiana, May 19–24, 2002* (2002), p. 1246.
14. T. Krajangsang, S. Inthisang, J. Sritharathikhun, A. Hongsingthong, A. Limmanee, S. Kittisontirak, P. Chinnavornrungsee, R. Phatthanakun, K. Sriprapha. An intrinsic amorphous silicon oxide and amorphous silicon stack passivation layer for crystalline silicon heterojunction solar cells. *Thin Solid Films* **628**, 107 (2017).
15. R.A. Street. *Hydrogenated Amorphous Silicon* (Cambridge Univ. Press, 2005) [ISBN: 9780521019347].
16. Y. Yan, M. Page, T.H. Wang, M.M. Al-Jassim, H.M. Branz, Q. Wang, Atomic structure and electronic properties of c-Si/a-Si:H heterointerfaces. *Appl. Phys. Lett.* **88**, 121925 (2006).
17. M.Dürr, U.Höfer. Hydrogen diffusion on silicon surfaces. *Prog. Surf. Sci.* **88**, 61 (2013).
18. J.P. Seif, D. Menda, A. Descoeudres, L. Barraud, O. Özdemir, C. Ballif, S. De Wolf. Asymmetric band offsets in silicon heterojunction solar cells: Impact on device performance. *J. Appl. Phys.* **120**, 054501 (2016).
19. U. Römer, R. Peibst, T. Ohrdes, B. Lim, J. Krügener, E. Bugiel, T. Wietler, R. Brendel. Recombination behavior and contact resistance of n^+ and p^+ poly-crystalline Si/mono-crystalline Si junctions, *Sol. Energ. Mat. Sol. Cell.* **131**, 85 (2014).
20. C. Becker, D. Amkreutz, T. Sontheimer, V. Preidel, D. Lockau, J. Haschke, L. Jogschies, C. Klimm, J. J. Merkel, P. Plocica, S. Steffens, B. Rech. Polycrystalline silicon thin-film solar cells: Status and perspectives. *Sol. Energy Mater. Sol. Cells* **119**, 112 (2013).
21. R. Peibst, U. Römer, Y. Larionova, M. Rienäcker, A. Merkle, N. Folchert, S. Reiter, M. Turcu, B. Min, J. Krügener, D. Tetzlaff, E. Bugiel, T. Wietler, R. Brendel. Working principle of carrier selective poly-Si/c-Si junctions: Is tunnelling the whole story? *Sol. Energy Mater. Sol. Cells* **158**, 60 (2016).
22. C.H. Seager, D.S. Ginley. Passivation of grain boundaries in polycrystalline silicon. *Appl. Phys. Lett.* **34**, 337 (1979).
23. A. Mimura, N. Konishi, K. Ono, J-I. Ohwada, Y. Hosokawa, Y-A. Ono, T. Suzuki, K. Miyata, H. Kawakami. High performance low-temperature poly-Si n-channel TFTs for LCD. *IEEE Trans. Electron Devices* **36**, 351 (1989).
24. N. Sridhar, D.D.L. Chung, W.A. Anderson, J. Coleman. Polysilicon films of high photoresponse, obtained by vacuum annealing of aluminum capped hydrogenated amorphous silicon. *J. Appl. Phys.* **78**, 7304 (1995).
25. J.A. Peck, P. Zonooz, D. Curreli, G.A. Panici, B.E. Jurczyk, D.N. Ruzic. High deposition rate nanocrystalline and amorphous silicon thin film production via surface wave plasma source. *Surf. Coat. Technol.* **325**, 370 (2017).
26. S. Honda, T. Mates, B. Rezek, A. Fejfar, J. Kočka. Microscopic study of the H_2O vapor treatment of the silicon grain boundaries. *J. Non-Cryst. Sol.* **354**, 2310 (2008).
27. S.A. Hadi, P. Hashemi, A. Nayfeh, J.L. Hoyt. Thin film a-Si/c-$Si_{1-x}Ge_x$/c-Si heterojunction solar cells: Design and material quality requirements. *ECS Trans.* **41**, 3 (2011).
28. E. Kadri, M. Krichen, A.B. Arab. Analytical method for the analysis of thin SiGe/Si solar cells with front surface field. *Opt. Quant. Electron.* **48**, 305 (2016).
29. E. Kadri, K. Dhahri, A. Zaafouri, M. Krichen, M. Rasheed, K. Khirouni, R. Barillé. ac conductivity and dielectric behavior of thin films synthesized by molecular beam epitaxial method. *J. Alloy. Compd.* **705**, 708 (2017).
30. A. Podolian, A. Nadtochiy, O. Korotchenkov, B. Romanyuk, V. Melnik, V. Popov. Enhanced photoresponse of Ge/Si nanostructures by combining amorphous silicon deposition and annealing. *J. Appl. Phys.* **124**, 095703 (2018).
31. M.Ya. Valakh, P.M. Lytvyn, A.S. Nikolenko, V.V. Strelchuk, Z.F. Krasilnik, D.N. Lobanov, A.V. Novikov. Gigantic uphill diffusion during self-assembled growth of Ge

quantum dots on strained SiGe sublayers. *Appl. Phys. Lett.* **96**, 141909 (2010).

32. A.V. Shah, H. Schade, M. Vanecek, J. Meier, E. Vallat-Sauvain, N. Wyrsch, U. Kroll, C. Droz, J. Bailat. Thin-film silicon solar cell technology. *Prog. Photovolt. Res. Appl.* **12**, 113 (2004).
33. J. Humlicek, F. Lukes, E. Schmidt. Silicon-germanium alloys (Si_xGe_{1-x}). In *Handbook of Optical Constants of Solids*. Edited by E.D. Palik (Academic Press, 1998), Part 2, Subpart 2 [ISBN: 0-12-544422-2].
34. L. Kronik, Y. Shapira. Surface photovoltage phenomena: theory, experiment, and applications. *Surf. Sci. Rep.* **37**, 1 (1999).
35. C.G.V. de Walle, R.M. Martin. Theoretical calculations of heterojunction discontinuities in the Si/Ge system. *Phys. Rev. B* **34**, 5621 (1986).
36. O.V. Vakulenko, S.V. Kondratenko, A.S. Nikolenko, S.L. Golovinskiy, Yu.N. Kozyrev, M.Yu. Rubezhanska, A.I. Vodyanitsky. Photoconductivity spectra of Ge/Si heterostructures with Ge QDs. *Nanotechnology* **18**, 185401 (2007).
37. S. Tardon, R. Brüggemann. Characterization of the interface properties in a-Si:H/c-Si heterostructures by photoluminescence. *J. Phys. D* **43**, 115102 (2010).
38. T.F. Schulze, L. Korte, E. Conrad, M. Schmidt, B. Rech. Electrical transport mechanisms in a-Si:H/c-Si heterojunction solar cells. *J. Appl. Phys.* **107**, 023711 (2010).
39. A. Nadtochiy, O. Korotchenkov, B. Romanyuk, V. Melnik, V. Popov. Photovoltage improvements in Cz–Si by low-energy implantation of carbon ions. *Mater. Res. Express* **3**, 055017 (2016).

Received 01.11.18.
Translated from Ukrainian by O.I. Voitenko

В. Шмід, А. Подолян,
А. Надточій, О. Коротченков, Б. Романюк,
В. Мельник, В. Попов, О. Косуля

ФОТОЕЛЕКТРИЧНІ ВЛАСТИВОСТІ ПЛІВОК SiGe, ПОКРИТИХ ШАРАМИ АМОРФНОГО ТА ПОЛІКРИСТАЛІЧНОГО КРЕМНІЮ

Р е з ю м е

Виявлено, що тонкі шари аморфного та полікристалічного Si (відповідно a-Si та poly-Si), нанесені на поверхню $Ge_{0,25}Si_{0,75}$, суттєво зменшують величину негативної фото-ЕРС, відтворюваній у шарі $Ge_{0,25}Si_{0,75}$, нанесеному на підкладку кристалічного Si. У той самий час, при достатній глибині проникнення світла, що включає обидва нанесені шари та приповерхневу область підкладки Si, у проміжки часу, більші за ≈10–20 мкс після закінчення світлового імпульсу, спостерігається фото-ЕРС позитивного знака. Виявлено також, що насичення киснем шару a-Si в гетероструктурі a-Si/$Ge_{0,25}Si_{0,75}$/c-Si призводить до суттєвого зростання величини додатної складової сигналу фото-ЕРС (в 6 разів у наших експериментах). Такий ефект може бути використано для розробки ефективних сонячних елементів на основі гетероструктури a-Si/Ge_xSi_{1-x}/c-Si.